HHS Public Access

Author manuscript

Int J Cancer. Author manuscript; available in PMC 2021 October 15.

Published in final edited form as:

Int J Cancer. 2020 October 15; 147(8): 2253–2264. doi:10.1002/ijc.33040.

Oncogenic properties and signaling basis of the *PAX8-GLIS3* fusion gene

Thais Basili[1,*], **Higinio Dopeso**[1,*], **Sarah H. Kim**[2,*], **Lorenzo Ferrando**[3], **Fresia Pareja**[1], **Arnaud Da Cruz Paula**[2], **Edaise M. da Silva**[1], **Anthe Stylianou**[2], **Ana Maroldi**[2], **Caterina Marchiò**[4,5], **Brian P. Rubin**[6], **Mauro Papotti**[7], **Britta Weigelt**[1], **Carlos Gil Moreira Ferreira**[8,9], **José Roberto Lapa e Silva**[9], **Jorge S. Reis-Filho**[1,10]

[1]Department of Pathology, Memorial Sloan Kettering Cancer Center, New York, NY, USA

[2]Department of Surgery, Memorial Sloan Kettering Cancer Center, New York, NY, USA

[3]Department of Internal Medicine, University of Genoa, Genova, Italy

[4]Candiolo Cancer Institute, FPO-IRCCS, Candiolo, Italy

[5]Department of Medical Sciences, University of Turin, Torino, Italy

[6]Department of Pathology, Cleveland Clinic, Cleveland, OH, USA

[7]Department of Oncology, University of Turin, at Città della Salute Hospital, Torino, Italy

[8]Oncoclinicas Institute for Research and Education, Sao Paulo, Brazil

[9]Federal University of Rio de Janeiro, Rio de Janeiro, Brazil

[10]Human Oncology and Pathogenesis Program, Memorial Sloan Kettering Cancer Center, New York, NY, USA

Abstract

Hyalinizing trabecular tumors (HTTs) of the thyroid are rare and mostly benign epithelial neoplasms of follicular cell origin, which have recently been shown to be underpinned by the *PAX8-GLIS3* fusion gene. In this study we sought to investigate the potential oncogenic mechanisms of the *PAX8-GLIS3* fusion gene. Forced expression of PAX8-GLIS3 was found to increase proliferation, clonogenic potential and migration of human non-malignant thyroid (Nthy-ori 3–1) and embryonic kidney (HEK-293) cells. Moreover, in xenografts, Nthy-ori 3–1 PAX8-

Correspondence to: Jorge S. Reis-Filho, MD PhD FRCPath, Memorial Sloan Kettering Cancer Center, Department of Pathology; 1275 York Avenue, New York, NY 10065, USA; Phone: +1 212 639 8054, reisfilj@mskcc.org.

*These authors contributed equally to this work.

DATA ACCESSIBILITY

Data will be made available upon reasonable request.

ETHICAL STATEMENT

In vivo studies were cared in accordance to the guidelines approved by the Memorial Sloan Kettering (MSK) Institutional Animal Care and Use Committee and Research Animal Resource Center.

CONFLICTS OF INTEREST

JSR-F reports personal/consultancy fees from Goldman Sachs and REPARE Therapeutics, membership of the scientific advisory board of VolitionRx and Page. AI, and ad hoc membership of the advisory board of Ventana Medical Systems, Roche Tissue Diagnostics, Genentech, Roche and InVicro, outside the submitted work. CM has received personal/consultancy fees from Bayer, Roche, Daiichi Sankyo, and MSD, outside the scope of the present work. All other authors declare no conflicts of interest.

GLIS3 expressing cells generated significantly larger and more proliferative tumors compared to controls. These oncogenic effects were found to be mediated through activation of the Sonic Hedgehog (SHH) pathway. Targeting of smoothened (SMO), a key protein in the SHH pathway, using the small molecule inhibitor Cyclopamine partially reversed the increased proliferation, colony formation and migration in PAX8-GLIS3 expressing cells. Our data demonstrate that the oncogenic effects of the *PAX8-GLIS3* fusion gene are, at least in part, due to an increased activation of the SHH pathway.

Keywords

Hyalinizing trabecular tumor; thyroid; fusion gene; sonic hedgehog pathway

INTRODUCTION

Hyalinizing trabecular tumors (HTTs) are rare thyroid neoplasms derived from follicular cells[1], which are considered to be of low malignant potential, with the vast majority behaving in a benign fashion[2]. These neoplasms are histologically composed of polygonal and spindle follicular cells arranged in a trabecular pattern with prominent intratrabecular hyalinized stroma, and nuclei with frequent grooves and inclusions[3]. Given the histologic similarities of HTTs with a variety of malignant tumors, in particular papillary thyroid carcinoma (PTC) and in rare exceptions medullary carcinomas, misdiagnoses of HTT can be encountered[1, 3], leading to unnecessary treatments with significant side effects in this otherwise benign condition.

Pathognomonic fusion genes affecting *GLIS3* (GLI Similar 3) have recently been described in HTTs by Nikiforova et al[4] and independently confirmed by our group[5]. These fusion genes have been found in 98% (47/48) of the HTTs analyzed to date and are composed of exons 1–2 of *PAX8* (Paired-box 8) fused with exons 3–11, or less frequently exons 2–11, of *GLIS3*, resulting in retention of the zinc finger and C2H2 domains of *GLIS3*. *PAX8* is a member of the paired box family of transcription factors involved in embryogenesis and cellular differentiation playing an important role in thyroid development and thyroid-specific gene expression[6, 7]. *GLIS3* is a Kruppel-like zinc finger transcription factor that participates in proliferation, apoptosis, cellular differentiation and embryological development[8, 9], and is expressed in thyroid follicular cells under physiologic conditions[10]. Deficiency in *GLIS3* is associated with congenital hypothyroidism[8, 10]. The *PAX8-GLIS3* fusion genes results in overexpression of the 3′-portion of *GLIS3* mRNA containing the DNA-binding domains of these transcription factors[5].

Given the importance of PAX8 in thyroid development and its constitutive expression in thyroid follicular cells[11], we hypothesized that in the case of *PAX8-GLIS3* fusion gene, the *PAX8* promoter increases expression of *GLIS3* leading to acquisition of oncogenic properties and driving the tumorigenesis of HTTs. In this study, we sought to investigate the potential oncogenic properties of the *PAX8-GLIS3* fusion gene. Our functional *in vitro* studies revealed that forced expression of the PAX8-GLIS3 fusion protein in non-malignant cells of different lineages and in xenograft models results in the acquisition of oncogenic

properties and increased signaling via the Sonic Hedgehog (SHH) pathway. Pharmacologic inhibition of the SHH pathway was found to reverse, at least in part, the *PAX8-GLIS3* oncogenic properties, thereby establishing the role of the SHH pathway in the pathogenesis of HTTs.

MATERIAL AND METHODS

Cell lines

The origin-defective SV40 genome (SV-ori) immortalized Nthy-ori 3–1 (RRID: CVCL_2659; 90011609, Sigma Aldrich) cell line was certified by ECACC and HEK-293 (RRID: CVCL_0045, CRL-1573, ATCC) cell line was authenticated using short tandem repeat profiling at Memorial Sloan Kettering Cancer Center (MSKCC) Integrated Genomics Operation (IGO) within the last three years. Nthy-ori 3–1 cells were cultured in RPMI 1640 with 2mM Glutamine and 10% fetal bovine serum (FBS). HEK-293 cells were cultured in Dulbecco's modified Eagle's medium (DMEM) high glucose supplemented with 10% FBS and 1% penicillin/streptomycin, as previously described[12]. All cell lines were maintained in a 5% CO_2 atmosphere at 37°C. All experiments were performed with mycoplasma-free cells, tested using the PCR-based Universal Mycoplasma Detection kit (ATCC), as previously described[12].

Generation of stable cell lines

For HTT cell models, human wild-type (WT) *PAX8* (EX-F0597-Lv102), WT *GLIS3* (EX-H1586-Lv102) and *PAX8-GLIS3* containing exons 1–2 of *PAX8* and 3–11 of *GLIS3* (CS-H1586-Lv102–01) ORF expression clones were purchased from GeneCopoeia. A FLAG-HA tag was added to the C-terminus of individual clones by PCR with custom primers and subsequently cloned into a pCDH-EF1α-MCS-BGH-PGK-GFP-T2A-Puro cDNA Dual Promoter Cloning and Expression Lentivector (CD550A-1, System Biosciences) (primer pairs are listed in Supplementary Table 1). Empty vector (EV) was used as a control. The lentiviral particles were produced at MSKCC's Gene Editing & Screening Core Facility. Nthy-ori 3–1 and HEK-293 cells were transduced for 24 h with lentivirus and then selected for 5 days in puromycin (2 μg/ml; ThermoFisher Scientific). Transduction efficiency was confirmed by EGFP (enhanced green fluorescent protein) reporter expression (% of EGFP positive cells), qRT-PCR (quantitative reverse transcription polymerase chain reaction) and immunoblotting.

Viral titration

Cells were seeded in 24-well plates (50,000 cells/well). On the following day, the cells were transduced for 6 h with 5-fold serial dilutions (25–78125) of EV lentivirus stock. Cells were incubated for 72 h. Transduction efficiency was confirmed by the number of EGFP expressing cells or colonies.

RNA extraction and quantitative RT-PCR

Total RNA was extracted from cells using RNeasy Mini Kit (Qiagen) and reverse-transcribed into cDNA using SuperScript VILO Master Mix (ThermoFisher), according to the manufacturer's instructions. Quantitative TaqMan RT-PCR was performed for *PAX8*

(Hs00247586), *GLIS3* (Hs00541450 - exons 7 and 8), *GLI1* (Hs00171790) and *PTCH1* (Hs00181117) using the StepOnePlus Real-Time PCR System (ThermoFisher). All experiments were performed in triplicate, and expression data were normalized to GAPDH (Hs02786624), as previously described[13].

Differential gene expression analysis

RNA samples extracted from Nthy-ori 3–1 and HEK-293 cells were subjected to RNA-sequencing (RNA-seq) using validated protocols at MSKCC Integrated Genomics Operation (IGO)[14]. Analyses were performed in R environment using edgeR (v3.24.3)[15]. Gene expression analysis was carried out using DESeq2 Bioconductor package. Minimal pre-filtering was performed to remove genes with less than one read across all samples. Normalization was performed adjusting the statistical model for size factors and measured using the median ratio method[16]. Fold change and statistical significance were assessed for all pair-wise comparisons. *P*-values were adjusted for multiple comparisons using Benjamini-Hochberg false discovery rate[17]. For the expression profiles of the canonical pathways, the corresponding genes were retrieved from Sanchez-Vega et al[18]. Read counts were converted to Log_2-counts-per-million (logCPM) and the mean variance relationship was modelled with an empirical Bayes prior trend using Limma package[19]. Log_2 transformed values of each cell line sample were normalized using the corresponding EV. Gene Set Enrichment Analysis (GSEA) was performed using clusterprofile package[20]. We retrieved and interrogated H, C2 and C5 pathways sets, corresponding to hallmark set, curated sets and Go sets. To generate p-value associated with potential pathways enrichment, 1000 permutations were performed.

Protein extraction and western blotting

Standard western blotting was conducted as previously described[13]. Cells were rinsed, pelleted by centrifugation and solubilized in RIPA buffer (Thermo Scientific) with 5% Halt Protease and Phosphatase Inhibitor Cocktail (Thermo Scientific) and 2% 0.5 mM EDTA (Thermo Scientific). Extracts were centrifuged, and the supernatant was then recovered for SDS-PAGE.

Primary antibodies against FLAG M2 (1:1000, Sigma, F1804), PTCH1 (1:1000, Abcam, ab53715), GLI1 (1:500, Abcam, ab134906) and tubulin (1:1000, Cell Signaling, DM1A) were used. Conjugated anti-rabbit (1:10000, LI-COR, 926–68073) and anti-mouse (1:10000, LI-COR, 926–32212) secondary antibodies, were used and detected using the Odyssey Infrared Imaging System (LI-COR Biosciences). Protein expression was quantified using the LI-COR Image Studio Software, as previously described[13]. Experiments were performed in triplicate.

Proliferation assay

Cells were seeded in 96-well plates (1000 cells/well; n=6 for each cell line and condition). Proliferation rate was assessed using the Cell Titer-Blue Cell Viability Assay (Promega), as previously described[12]. Absorbance was detected with 560 nm excitation and 590 nm emission using a Victor X4 Multimode Plate Reader (PerkinElmer), as previously described[12, 13]. Experiments for each condition were performed in triplicate.

Scratch wound healing assay

Cells were seeded in 24-well plates at 90–95% confluence. On the following day, a scratch was made on the cell monolayer using a 1 ml pipette tip across the center of the well. Phase-contrast images were obtained at 0 h and 24 h following scratch wounding, using an EVOS XL Core Microscope (ThermoFisher Scientific). Wound area was measured using ImageJ, and the percent of wound closure was determined, as previously described[12, 13]. Experiments for each condition were performed in triplicate.

Time-lapse scratch wound healing assay

Cells were seeded in 24-well plates at 90–95% confluence. On the following day, a scratch was made on the cell monolayer using a 1 ml pipette tip across the center of the well. Time-lapse images were obtained every hour during the course of 24 h following scratch wounding, using a Zeiss Axio Observer Z1 microscope, utilizing a 5×0.15NA objective and a Hamamatsu Flash V3 cMOS camera. The motorized stage was calibrated to conduct tile-imaging of the portion of each well containing the scratch every hour. Stitched images were analyzed using ImageJ/FIJI employing a customized macro script. Sharpening and variance filters were used to segment the cells from the scratch and the area was measured and calculated for each timepoint. The percent of wound closure was determined as previously described[12, 13]. Experiments for each condition were performed in triplicates.

Colony formation assay

Cells were seeded in 6-well plates (500–100 cells/well). After 7 days, cells were fixed and stained using the sulforhodamine B (SRB) protocol as previously described[13]. In brief, cells were fixed at 4°C for 1 h using Trichloroacetic acid (Sigma). Cells were stained on a rocking platform for 30 min with 0.04% SRB in 1% acetic acid. Plates were imaged using a Zeiss Observer Z1 microscope, using a 5x/0.5NA objective and a Hamamatsu Flash V3 cMOS camera. Motorized stage was calibrated to conduct tile-imaging of the entirety of each well. Stitched images were analyzed in ImageJ/FIJI using a customized macro script. Gaussian and median filters were used to blur the image before colonies were detected by intensity threshold. Touching colonies were separated using a Watershed algorithm. Quantification of the number of colonies per well and colony size was performed using ImageJ. Experiments for each condition were performed in triplicate.

Xenograft model

Athymic (nu/nu; Envigo Laboratories) mice (n=6) were used for *in vivo* studies and were cared for in accordance to the guidelines approved by the Memorial Sloan Kettering (MSK) Institutional Animal Care and Use Committee and Research Animal Resource Center. Xenografts were generated by injecting 10 million Nthy-ori 3–1 cells with matrigel (50:50) subcutaneously in both flanks of a 6-week-old athymic female mice. Tumors were measured every two days using calipers and volume was calculated using the formula: length x width^2 × 0.52. Body weight and clinical signs were also assessed. At the end of the study, the tumors were collected for histological and immunohistochemical analysis.

Immunohistochemistry

Tissues from xenografts were fixed in 10% neutral buffered formalin (Sigma-Aldrich) and subsequently embedded in paraffin. Four-micrometer-thick sections were prepared using a Leica RM 2155 rotary microtome. Immunohistochemistry was performed using Discovery Ultra (Roche) with CC1 Heat retrieval solution and Optiview DAB IHC Detection kit (760–700) with monoclonal antibody against MUC1 (1:100, MRQ-17; Cell Marque, 290-M-15) and ENO2 (1:3, NSE, MRQ-55; Cell Marque, 760-4786).

Reagents

The smoothened inhibitor, Cyclopamine (Selleckchem, S1146) was resuspended in DMSO and used in a dose-response proliferation assay at concentrations of 10, 20 and 40 μM and in proliferation, clonogenic and scratch wound healing assays at a concentration of 10 μM[21]. The human recombinant SHH Protein (Sigma-Aldrich, GF174) was resuspended in PBS and employed in the proliferation and scratch wound healing assays at a concentration of 1 μg/ml. Cells were treated for 6 hours with the proteasome inhibitor MG-132 (Sigma-Aldrich, M7449) at 10 μM prior to cells lysis for western blotting.

Statistical analysis

Statistical analysis was performed using Prism 7 (GraphPad). Two-tailed student's t-test was employed for the comparison of means in parametric data. A P value <0.05 was considered significant.

RESULTS

PAX8-GLIS3 expression results in the acquisition of oncogenic properties *in vitro*

To study the effects of PAX8-GLIS3 expression *in vitro*, and given that HTT cell lines are not available, we first generated HTT relevant cell models by forced expression of the *PAX8-GLI3* fusion gene in Nthy-ori 3–1 immortalized human thyroid follicular epithelial cells, the putative cell of origin of HTTs[1], and in HEK-293 cells. In addition, we generated Nthy-ori 3–1 and HEK-293 cells with forced expression of WT PAX8 or WT GLIS3 as controls.

We confirmed the expression of our constructs at the mRNA and protein levels by qRT-PCR and western blotting, respectively (Figs. 1a–1b). For qRT-PCR, we used a probe designed to anneal to exons 7 and 8 of *GLIS3*, capturing the *GLIS3* transcript present in the fusion gene in addition to endogenous *GLIS3*.

Forced expression of PAX8-GLIS3 protein in Nthy-ori 3–1 and HEK-293 cells led to a significant increase in cellular proliferation (Fig. 2a), in the number of colonies in a colony formation assay (Fig. 2b) and in cellular migration (Fig. 2c) compared to Control and PAX8 expressing cells, and to significantly higher cellular proliferation and/or migration rates than those observed in cells expressing GLIS3 (Fig. 2). In time-lapse video imaging of the wound healing assay using both Nthy-ori 3–1 and HEK-293 cells (Supplementary Videos), we consistently observed a significantly increased migration rate of cells expressing PAX8-GLIS3 when compared to control cells (Fig. 2d).

These findings are consistent with the notion that the *PAX8-GLIS3* fusion gene has oncogenic properties *in vitro*, which, at least in part, can be recapitulated by forced expression of GLIS3.

PAX8-GLIS3 expression results in Sonic Hedgehog pathway activation

GLIS3 regulates gene transcription by binding specific DNA sequences referred to as GLIS-binding sites (GLIS-BS) in promoter regulatory regions of target genes[22], acting downstream of the SHH pathway[9]. The latter plays an important role in regulating cell growth, differentiation and tissue patterning during normal embryogenesis[23]. Deregulated SHH signaling has been found in human cancer, such as gastric, breast, lung, skin, prostate and thyroid cancers[23–26]. Given that *GLIS3* is a component of the SHH pathway, which plays pivotal roles in tumorigenesis, we posited that the *PAX8-GLIS3* fusion gene would exert its oncogenic effects in our cell models through activation of the SHH pathway.

To determine whether the *PAX8-GLIS3* fusion gene would result in activation of the SHH pathway, we assessed the gene and protein expression levels of the SHH targets PTCH1 and GLI1 in our cell models upon forced expression of the PAX8-GLIS3 fusion protein, GLIS3, PAX8 and Control (Figs. 3a–3b). Using qRT-PCR and western blotting, we observed significantly increased *PTCH1 and GLI1* mRNA and protein levels in Nthy-ori 3–1 and HEK-293 cells upon PAX8-GLIS3 expression when compared to WT PAX8 and control (Figs. 3a–3b). As expected, expression of GLIS3 also resulted in higher levels of *PTCH1* and/or *GLI1* as compared to those in PAX8 and control although not as high as with the PAX8-GLIS3 fusion protein (Figs. 3a–3b).

We also assessed whether treatment with the SHH ligand protein would lead to enhanced proliferation and migration of parental cells. Upon treatment with SHH protein, significantly increased proliferation and migration rates of both Nthy-ori 3–1 and HEK-293 parental cells when compared to controls was observed (Figs. 3c–3d), supporting the notion that SHH pathway activation is sufficient to enhance oncogenic properties *in vitro.*

When activated, the SHH pathway induces the transcription of GLI-targets and inhibits the degradation of PTCH1 and GLI1 by the proteasome simultaneously, causing stabilization of the proteins[27, 28]. Upon treatment with the proteasome inhibitor MG-132 for 6 hours prior to cell lysis for western blotting, we observed increased protein expression of both GLI-targets, although more evident in PTCH1 (Supplementary Fig. 1), in both cell models. These findings support the notion that proteasome degradation of PTCH1 and GLI1 is maintained as a mechanism of SHH pathway regulation in the cell models employed.

Inhibition of the SHH pathway can reverse oncogenic properties downstream of *PAX8-GLIS3*

The SHH pathway has been shown to be an important oncogenic driver in different cancer types, such as basal cell carcinoma and medulloblastoma[29, 30]. Additionally, antagonists targeting smoothened (SMO) and GLI1, key signaling components of the SHH pathway, are now FDA approved for the treatment of basal cell carcinomas[29, 31, 32]. Given the activation of the SHH pathway upon forced expression of *PAX8-GLIS3* fusion gene observed in our *in vitro* models, we assessed whether pharmacologic inhibition of the SHH pathway using

Cyclopamine, a highly specific inhibitor of SMO, would result in reversal of the oncogenic properties observed in the cells expressing PAX8-GLIS3 fusion protein.

To define the minimum concentration of Cyclopamine required to suppress enhanced SHH pathway activity, a dose-dependent proliferation assay was performed using empty vector (Control) and PAX8-GLIS3 expressing Nthy-ori 3–1 and HEK-293 cells. A significant decrease in the proliferation of PAX8-GLIS3 Nthy-ori 3–1 and HEK-239 cells was observed upon Cyclopamine treatment at 10 μM (Fig. 4a) and 20 μM. In contrast, the proliferation rate of Control, PAX8 or GLIS3 expressing cells was not significantly affected upon treatment with 10 μM Cyclopamine. These results indicate that Cyclopamine at 10 μM is sufficient to suppress the increased SHH pathway activity of cells expressing the PAX8-GLIS3 fusion gene but not to inhibit the basal level of SHH pathway activity present in control cells (Supplementary Fig. 2).

Consistent with the decrease in proliferation we observed upon treatment of our Nthy-ori 3–1 and HEK-293 cells models with Cyclopamine at 10μM (Fig. 4a), we observed a significant reversal of the increased colony formation (Fig. 4b) and cell migration (Fig. 4c) in cells expressing PAX8-GLIS3 and GLIS3 as compared to cells expressing PAX8 or Control.

Taken together, these results implicate the SHH pathway in the oncogenic activity observed in cells stably transduced with the fusion *PAX8-GLIS3*, providing further evidence for the underlying biological basis and the likely pathogenic role of this fusion gene in HTTs.

PAX8-GLIS3 expression results in acquisition of HTT features

To assess whether PAX8-GLIS3 expression promotes tumorigenicity, we generated xenografts by injecting the transduced Nthy-ori 3–1 cells into athymic mice. Over the course of 23 days, we observed a significantly increased tumor volume in xenografts from Control, PAX8 and GLIS3 expressing cells (Fig. 5a).

Histologically, xenografts displayed a solid architecture with extensive necrosis, nuclear pleomorphism and frequent mitoses. Hyaline material was observed in xenografts of all conditions tested. PAX8-GLIS3 xenografts displayed a higher mitotic rate than xenografts from other conditions (p=0.00028, Fig 5b). Immunohistochemically, MUC1 and Gamma-enolase (ENO2), also known as neuron-specific enolase (NSE), which are expressed in other epithelial/ neuroepithelial malignancies, including a subset of thyroid cancers, but not in HTTs[33–36], were found to be expressed at significantly lower levels in xenografts from PAX8-GLIS3 expressing cells than in xenografts from Control, PAX8 or GLIS3 expressing cells (Fig. 5c).

Taken together, these results demonstrate that our xenograft model derived from Nthy-ori 3–1 PAX8-GLIS3 expressing cells recapitulate some of the cardinal immunohistochemical features of HTT tumors.

Differential gene expression analysis between the different conditions of both Nthy-ori 3–1 and HEK-293 cells also revealed an enrichment for extracellular matrix and/or differentiation markers associated with HTTs in PAX8-GLIS3 Nthy-ori 3–1 and HEK-293 expressing cells (Fig. 5d), consistent with the notion that PAX8-GLIS3 expression likely

plays a causative role in the acquisition of some of the cardinal phenotypic characteristics of HTTs. Additionally, this analysis revealed an enrichment of SHH pathway genes, including *PTCH1*, *PTCH2* and *HHIP* in PAX8-GLIS3 expressing cells as compared to Control, PAX8 and GLIS3 expressing cells in both cell lines (Fig. 5d). We next performed an exploratory, hypothesis generating analysis to identify pathways in addition to SHH potentially activated by the expression PAX8-GLIS3 fusion gene. These analyses failed to identify any other cancer-related canonical signaling pathway, as defined by the annotations employed by Sanchez-Vega et al[18] or by Gene Set Enrichment Analysis, to be significantly enriched in cells expressing PAX8-GLIS3 in comparison to cells expressing PAX8 or normal thyroid tissues (data not shown).

DISCUSSION

Here we present a functional analysis of *PAX8-GLIS3* fusion gene in HTTs, a genetic rearrangement that has recently been shown to be pathognomonic of these rare thyroid neoplasms[4, 5]. We provide evidence that forced expression of the *PAX8-GLIS3* fusion gene results in the acquisition of oncogenic properties *in vitro*, including increased proliferation, colony formation and migration capacity. This increase in oncogenic potential is reversed by Cyclopamine, a specific inhibitor of the SHH pathway, supporting the notion that activation of the SHH pathway is at least in part responsible for the oncogenic properties of the *PAX8-GLIS3* fusion gene.

PAX8 is a transcription factor and interacts with specific DNA sequences via its paired domain[37]. PAX8 also appears to control the expression of various genes that play key roles in the function of thyroid follicular cells, and loss-of-function mutations in *PAX8* lead to thyroid dysgenesis[11]. Furthermore, dysregulated *PAX8* expression has been implicated in thyroid carcinomas[11, 38]. *GLIS3*, a member of the GLI-Similar zinc finger protein family, encodes for a nuclear protein with five zinc finger domains[8] and has a known role in transcriptional activation and repression during embryogenesis[39]. In adults, GLIS3 acts downstream of thyroid-stimulating hormone (TSH) and TSH receptor (TSHR), indispensable for the biosynthesis and proliferation of thyroid follicular cells[10]. Aberrant expression of GLIS3 has been described in different types of cancer, notably breast cancer, glioblastomas and renal cell carcinomas[40–43]. Apart from the aberrant expression levels, a fusion gene involving cleft lip and palate transmembrane protein 1-like (*CLPTM1L*) and *GLIS3* genes has been reported in cases of fibrolamellar hepatocellular carcinoma[44]. Based on our findings and on previous reports[4, 5], in the *PAX8-GLIS3* fusion, the promoter of *PAX8*, normally expressed in thyroid cells, increases the expression of exons 3–11 of *GLIS3,* which contain the zinc finger C2H2 domain. This leads to constitutive activation of *GLIS3*, resulting in cellular properties essential for tumorigenesis.

Gene and protein expression analysis revealed that expression of the PAX8-GLIS3 fusion results in increased signaling via the SHH pathway by upregulation of key members of the pathway, PTCH1 and GLI1. These results were corroborated by a gene expression analysis of SHH pathway genes in which *PTCH1*, *PTCH2*, *HHIP*, *IHH*, *GLI1* and *GLI2* were found to be co-expressed with the *PAX8-GLIS3* fusion gene. In addition, our hypothesis generating analysis did not reveal a robust and significant enrichment of the other signaling

pathways, supporting the notion that the effects caused by the expression of the fusion protein in our cell models are likely predominantly driven by SHH pathway. SHH signaling pathway plays an essential role during vertebrate embryonic development and tumorigenesis[45]. It is activated during development for intercellular communication and is important for the organogenesis in mammals, as well as in regeneration and homeostasis[23]. Basal cell carcinomas and medulloblastomas harbor high frequencies of activating mutations of the SHH pathway and respond to treatment with SMO inhibitors[46]. Presently, there are several SHH inhibitors being investigated in clinical trials with SMO as the principal target, such as Cyclopamine[23, 47]. In our study, *in vitro* analyses have demonstrated that the oncogenic properties induced by the expression of the *PAX8-GLIS3* fusion could be reversed through the inhibition of SHH pathway with Cyclopamine, thus corroborating the notion that SHH signaling pathway activation plays an important role in HTTs. These results warrant further testing of SMO inhibitors, such as Cyclopamine or Vismodegib, as potential therapeutic strategies for patients with HTTs that may not be amenable to surgical resection.

Xenografts can be a powerful tool to provide valuable insights into cancer development, providing an opportunity to evaluate malignant transformation, invasion, metastasis and drug response as well as the process of tumorigenesis in an *in vivo* setting[48, 49]. Here, we observed that xenografts derived from PAX8-GLIS3 expressing Nthy-ori 3–1 cells displayed higher tumor growth and proliferative activity than xenografts derived from empty vector (Control), PAX8 and GLIS3 expressing cells. In addition, we have observed that xenografts derived from PAX8-GLIS3 expressing Nthy-ori 3–1 cells harbored immunophenotypic characteristics similar to those of human HTTs.

Our study also has limitations due to the lack of representative cell models derived from human HTTs. We, therefore, introduced the *PAX8-GLIS3* fusion into Nthy-ori 3–1 (i.e. thyroid follicular cells) and HEK-293 cell lines. Although HEK-293 cells are not representative of the likely cell of origin, *PAX8-GLIS3* fusion gene expression resulted in the acquisition of oncogenic properties and SHH pathway activation similar to those observed in Nthy-ori 3–1 cells. Whilst the expression of the fusion gene in our constructs is under the control of EF1α promoter rather than the PAX8, we are confident that the primary pathogenic mechanism underlying the *PAX8-GLIS3* fusion gene (i.e. constitutive activation of *GLIS3*) is captured in our cell models. We confirmed the expression of the fusion by qRT-PCR and immunoblotting under the control of this promoter. Additionally, we observed increased expression of downstream targets of the SHH pathway, further validating the biologic relevance of our models. Finally, in the present study, we have focused on the *PAX8-GLIS3* fusion gene and did not study the functionality of the *PAX8-GLIS1* fusion, which was found to be present in 1 out of the 14 HTTs reported by Nikiforova et al[4]. Considering the similarities between the *PAX8-GLIS3* and *PAX8-GLIS1* fusion genes, however, it would be reasonable to hypothesize that these fusions may co-opt similar oncogenic pathways. Further studies to investigate the mechanism of the *PAX8-GLIS1* fusion gene are warranted.

Despite these limitations, here we provide evidence that the *PAX8-GLIS3* fusion gene confers oncogenic properties *in vitro* and *in vivo* and that this effect is mediated at least in part via activation of the SHH signaling pathway. Our findings implicate a central role of

GLIS3 rearrangements in HTTs and provide further evidence that PAX8-GLIS3 should be included in the diagnostic work up of these rare tumors. Furthermore, our results provide evidence to support the potential therapeutic benefit of SHH antagonists in the treatment of HTTs.

Supplementary Material

Refer to Web version on PubMed Central for supplementary material.

ACKNOWLEDGEMENTS

We thank the Gene Editing & Screening, Molecular Cytology and Antitumor Assessment Core Facilities at MSKCC. JSR-F is funded in part by a Breast Cancer Research Foundation fellowship. BW is funded in part by a Cycle for Survival grant. FP is partly funded by a National Institutes of Health K12 CA184746 grant. Research reported in this publication was partly funded by a Cancer Center Support Grant of the National Institutes of Health/ National Cancer Institute (grant No P30CA008748). The content is solely the responsibility of the authors and does not necessarily represent the official views of the National Institutes of Health.

List of abbreviations:

HTT	Hyalinizing trabecular tumor
PTC	Papillary thyroid carcinoma
SHH	Sonic Hedgehog

REFERENCES

1. Jones DJ, Kieliszak CR, Patel SS, Selinsky CR. Hyalinizing trabecular tumor of the thyroid gland and its significant diagnostic issue. Thyroid Res 2017;10: 7. [PubMed: 29051791]
2. Papotti M VM. Hyalinizing trabecular tumor In: Lloyd RV OR, Klöppel G, Rosai J. WHO classification of tumors of endocrine organs ed.: Lyon: IARC Press, 2017: 73–4.
3. Jang H, Park CK, Son EJ, Kim EK, Kwak JY, Moon HJ, Yoon JH. Hyalinizing trabecular tumor of the thyroid: diagnosis of a rare tumor using ultrasonography, cytology, and intraoperative frozen sections. Ultrasonography 2016;35: 131–9. [PubMed: 26639939]
4. Nikiforova MN, Nikitski AV, Panebianco F, Kaya C, Yip L, Williams M, Chiosea SI, Seethala RR, Roy S, Condello V, Santana-Santos L, Wald AI, et al. GLIS Rearrangement is a Genomic Hallmark of Hyalinizing Trabecular Tumor of the Thyroid Gland. Thyroid 2019;29: 161–73. [PubMed: 30648929]
5. Marchio C, Da Cruz Paula A, Gularte-Merida R, Basili T, Brandes A, da Silva EM, Silveira C, Ferrando L, Metovic J, Maletta F, Annaratone L, Pareja F, et al. PAX8-GLIS3 gene fusion is a pathognomonic genetic alteration of hyalinizing trabecular tumors of the thyroid. Mod Pathol 2019;32: 1734–43. [PubMed: 31273314]
6. Xiang L, Kong B. PAX8 is a novel marker for differentiating between various types of tumor, particularly ovarian epithelial carcinomas. Oncol Lett 2013;5: 735–8. [PubMed: 23425942]
7. Pasca di Magliano M, Di Lauro R, Zannini M. Pax8 has a key role in thyroid cell differentiation. Proc Natl Acad Sci U S A 2000;97: 13144–9.
8. Jetten AM. GLIS1–3 transcription factors: critical roles in the regulation of multiple physiological processes and diseases. Cell Mol Life Sci 2018;75: 3473–94. [PubMed: 29779043]
9. Kim YS, Nakanishi G, Lewandoski M, Jetten AM. GLIS3, a novel member of the GLIS subfamily of Kruppel-like zinc finger proteins with repressor and activation functions. Nucleic Acids Res 2003;31: 5513–25. [PubMed: 14500813]

10. Kang HS, Kumar D, Liao G, Lichti-Kaiser K, Gerrish K, Liao XH, Refetoff S, Jothi R, Jetten AM. GLIS3 is indispensable for TSH/TSHR-dependent thyroid hormone biosynthesis and follicular cell proliferation. J Clin Invest 2017;127: 4326–37. [PubMed: 29083325]
11. Rosignolo F, Sponziello M, Durante C, Puppin C, Mio C, Baldan F, Di Loreto C, Russo D, Filetti S, Damante G. Expression of PAX8 Target Genes in Papillary Thyroid Carcinoma. PLoS One 2016;11: e0156658.
12. Pareja F, Brandes AH, Basili T, Selenica P, Geyer FC, Fan D, Da Cruz Paula A, Kumar R, Brown DN, Gularte-Merida R, Alemar B, Bi R, et al. Loss-of-function mutations in ATP6AP1 and ATP6AP2 in granular cell tumors. Nat Commun 2018;9: 3533. [PubMed: 30166553]
13. Kim SH, Da Cruz Paula A, Basili T, Dopeso H, Bi R, Pareja F, da Silva EM, Gularte-Merida R, Sun Z, Fujisawa S, Smith CG, Ferrando L, et al. Identification of recurrent FHL2-GLI2 oncogenic fusion in sclerosing stromal tumors of the ovary. Nat Commun 2020;11: 44. [PubMed: 31896750]
14. Geyer FC, Li A, Papanastasiou AD, Smith A, Selenica P, Burke KA, Edelweiss M, Wen HC, Piscuoglio S, Schultheis AM, Martelotto LG, Pareja F, et al. Recurrent hotspot mutations in HRAS Q61 and PI3K-AKT pathway genes as drivers of breast adenomyoepitheliomas. Nat Commun 2018;9: 1816. [PubMed: 29739933]
15. Robinson MD, McCarthy DJ, Smyth GK. edgeR: a Bioconductor package for differential expression analysis of digital gene expression data. Bioinformatics 2010;26: 139–40. [PubMed: 19910308]
16. Anders S, Huber W. Differential expression analysis for sequence count data. Genome Biol 2010;11: R106. [PubMed: 20979621]
17. Benjamini Y, Drai D, Elmer G, Kafkafi N, Golani I. Controlling the false discovery rate in behavior genetics research. Behav Brain Res 2001;125: 279–84. [PubMed: 11682119]
18. Sanchez-Vega F, Mina M, Armenia J, Chatila WK, Luna A, La KC, Dimitriadoy S, Liu DL, Kantheti HS, Saghafinia S, Chakravarty D, Daian F, et al. Oncogenic Signaling Pathways in The Cancer Genome Atlas. Cell 2018;173: 321–37 e10.
19. Ritchie ME, Phipson B, Wu D, Hu Y, Law CW, Shi W, Smyth GK. limma powers differential expression analyses for RNA-sequencing and microarray studies. Nucleic Acids Res 2015;43: e47.
20. Yu G, Wang LG, Han Y, He QY. clusterProfiler: an R package for comparing biological themes among gene clusters. OMICS 2012;16: 284–7. [PubMed: 22455463]
21. Sun Y, Guo W, Ren T, Liang W, Zhou W, Lu Q, Jiao G, Yan T. Gli1 inhibition suppressed cell growth and cell cycle progression and induced apoptosis as well as autophagy depending on ERK1/2 activity in human chondrosarcoma cells. Cell Death Dis 2014;5: e979.
22. Kang HS, Kim YS, ZeRuth G, Beak JY, Gerrish K, Kilic G, Sosa-Pineda B, Jensen J, Pierreux CE, Lemaigre FP, Foley J, Jetten AM. Transcription factor Glis3, a novel critical player in the regulation of pancreatic beta-cell development and insulin gene expression. Mol Cell Biol 2009;29: 6366–79. [PubMed: 19805515]
23. Carballo GB, Honorato JR, de Lopes GPF, Spohr T. A highlight on Sonic hedgehog pathway. Cell Commun Signal 2018;16: 11. [PubMed: 29558958]
24. Samadani AA, Akhavan-Niaki H. Interaction of sonic hedgehog (SHH) pathway with cancer stem cell genes in gastric cancer. Med Oncol 2015;32: 48. [PubMed: 25636508]
25. Noman AS, Uddin M, Chowdhury AA, Nayeem MJ, Raihan Z, Rashid MI, Azad AK, Rahman ML, Barua D, Sultana A, Shirin A, Ferdous J, et al. Serum sonic hedgehog (SHH) and interleukin-(IL-6) as dual prognostic biomarkers in progressive metastatic breast cancer. Sci Rep 2017;7: 1796. [PubMed: 28496132]
26. Rashid FA, Mansoor Q, Tabassum S, Aziz H, Arfat WO, Naoum GE, Ismail M, Farooqi AA. Signaling cascades in thyroid cancer: Increasing the armory of archers to hit bullseye. J Cell Biochem 2018;119: 3798–808. [PubMed: 29243843]
27. Chen XL, Chinchilla P, Fombonne J, Ho L, Guix C, Keen JH, Mehlen P, Riobo NA. Patched-1 proapoptotic activity is downregulated by modification of K1413 by the E3 ubiquitin-protein ligase Itchy homolog. Mol Cell Biol 2014;34: 3855–66. [PubMed: 25092867]
28. Schrader EK, Harstad KG, Holmgren RA, Matouschek A. A three-part signal governs differential processing of Gli1 and Gli3 proteins by the proteasome. J Biol Chem 2011;286: 39051–8.

29. Epstein EH. Basal cell carcinomas: attack of the hedgehog. Nat Rev Cancer 2008;8: 743–54. [PubMed: 18813320]
30. Yoon JW, Gilbertson R, Iannaccone S, Iannaccone P, Walterhouse D. Defining a role for Sonic hedgehog pathway activation in desmoplastic medulloblastoma by identifying GLI1 target genes. Int J Cancer 2009;124: 109–19. [PubMed: 18924150]
31. Raffel C, Jenkins RB, Frederick L, Hebrink D, Alderete B, Fults DW, James CD. Sporadic medulloblastomas contain PTCH mutations. Cancer Res 1997;57: 842–5. [PubMed: 9041183]
32. Teglund S, Toftgard R. Hedgehog beyond medulloblastoma and basal cell carcinoma. Biochim Biophys Acta 2010;1805: 181–208. [PubMed: 20085802]
33. Eminaga O, Wei W, Hawley SJ, Auman H, Newcomb LF, Simko J, Hurtado-Coll A, Troyer DA, Carroll PR, Gleave ME, Lin DW, Nelson PS, et al. MUC1 Expression by Immunohistochemistry Is Associated with Adverse Pathologic Features in Prostate Cancer: A Multi-Institutional Study. PLoS One 2016;11: e0165236.
34. Kaleem Z, Davila RM. Hyalinizing trabecular adenoma of the thyroid. A report of two cases with cytologic, histologic and immunohistochemical findings. Acta Cytol 1997;41: 883–8. [PubMed: 9167720]
35. Li J, Yang GZ, Gao LX, Yan WX, Jin H, Li L. Hyalinizing trabecular tumor of the thyroid: Case report and review of the literature. Exp Ther Med 2012;3: 1015–7. [PubMed: 22970009]
36. Vizin T, Kos J. Gamma-enolase: a well-known tumour marker, with a less-known role in cancer. Radiol Oncol 2015;49: 217–26. [PubMed: 26401126]
37. Pellizzari L, Fabbro D, Lonigro R, Di Lauro R, Damante G. A network of specific minor-groove contacts is a common characteristic of paired-domain-DNA interactions. Biochem J 1996;315 (Pt 2): 363–7. [PubMed: 8615801]
38. Bishop JA, Sharma R, Westra WH. PAX8 immunostaining of anaplastic thyroid carcinoma: a reliable means of discerning thyroid origin for undifferentiated tumors of the head and neck. Hum Pathol 2011;42: 1873–7. [PubMed: 21663937]
39. Dimitri P. The role of GLIS3 in thyroid disease as part of a multisystem disorder. Best Pract Res Clin Endocrinol Metab 2017;31: 175–82. [PubMed: 28648506]
40. Rami F, Baradaran A, Kahnamooi MM, Salehi M. Alteration of GLIS3 gene expression pattern in patients with breast cancer. Adv Biomed Res 2016;5: 44. [PubMed: 27099857]
41. Cooper LA, Gutman DA, Long Q, Johnson BA, Cholleti SR, Kurc T, Saltz JH, Brat DJ, Moreno CS. The proneural molecular signature is enriched in oligodendrogliomas and predicts improved survival among diffuse gliomas. PLoS One 2010;5: e12548.
42. Chou CK, Tang CJ, Chou HL, Liu CY, Ng MC, Chang YT, Yuan SF, Tsai EM, Chiu CC. The Potential Role of Kruppel-Like Zinc-Finger Protein Glis3 in Genetic Diseases and Cancers. Arch Immunol Ther Exp (Warsz) 2017;65: 381–9. [PubMed: 28523428]
43. Yusenko MV, Kovacs G. Identifying CD82 (KAI1) as a marker for human chromophobe renal cell carcinoma. Histopathology 2009;55: 687–95. [PubMed: 20002769]
44. Xu L, Hazard FK, Zmoos AF, Jahchan N, Chaib H, Garfin PM, Rangaswami A, Snyder MP, Sage J. Genomic analysis of fibrolamellar hepatocellular carcinoma. Hum Mol Genet 2015;24: 50–63. [PubMed: 25122662]
45. Jiang J, Hui CC. Hedgehog signaling in development and cancer. Dev Cell 2008;15: 801–12. [PubMed: 19081070]
46. Shou Y, Robinson DM, Amakye DD, Rose KL, Cho YJ, Ligon KL, Sharp T, Haider AS, Bandaru R, Ando Y, Geoerger B, Doz F, et al. A five-gene hedgehog signature developed as a patient preselection tool for hedgehog inhibitor therapy in medulloblastoma. Clin Cancer Res 2015;21: 585–93. [PubMed: 25473003]
47. Batsaikhan BE, Yoshikawa K, Kurita N, Iwata T, Takasu C, Kashihara H, Shimada M. Cyclopamine decreased the expression of Sonic Hedgehog and its downstream genes in colon cancer stem cells. Anticancer Res 2014;34: 6339–44. [PubMed: 25368233]
48. Richmond A, Su Y. Mouse xenograft models vs GEM models for human cancer therapeutics. Dis Model Mech 2008;1: 78–82. [PubMed: 19048064]
49. Lee NP, Chan CM, Tung LN, Wang HK, Law S. Tumor xenograft animal models for esophageal squamous cell carcinoma. J Biomed Sci 2018;25: 66. [PubMed: 30157855]

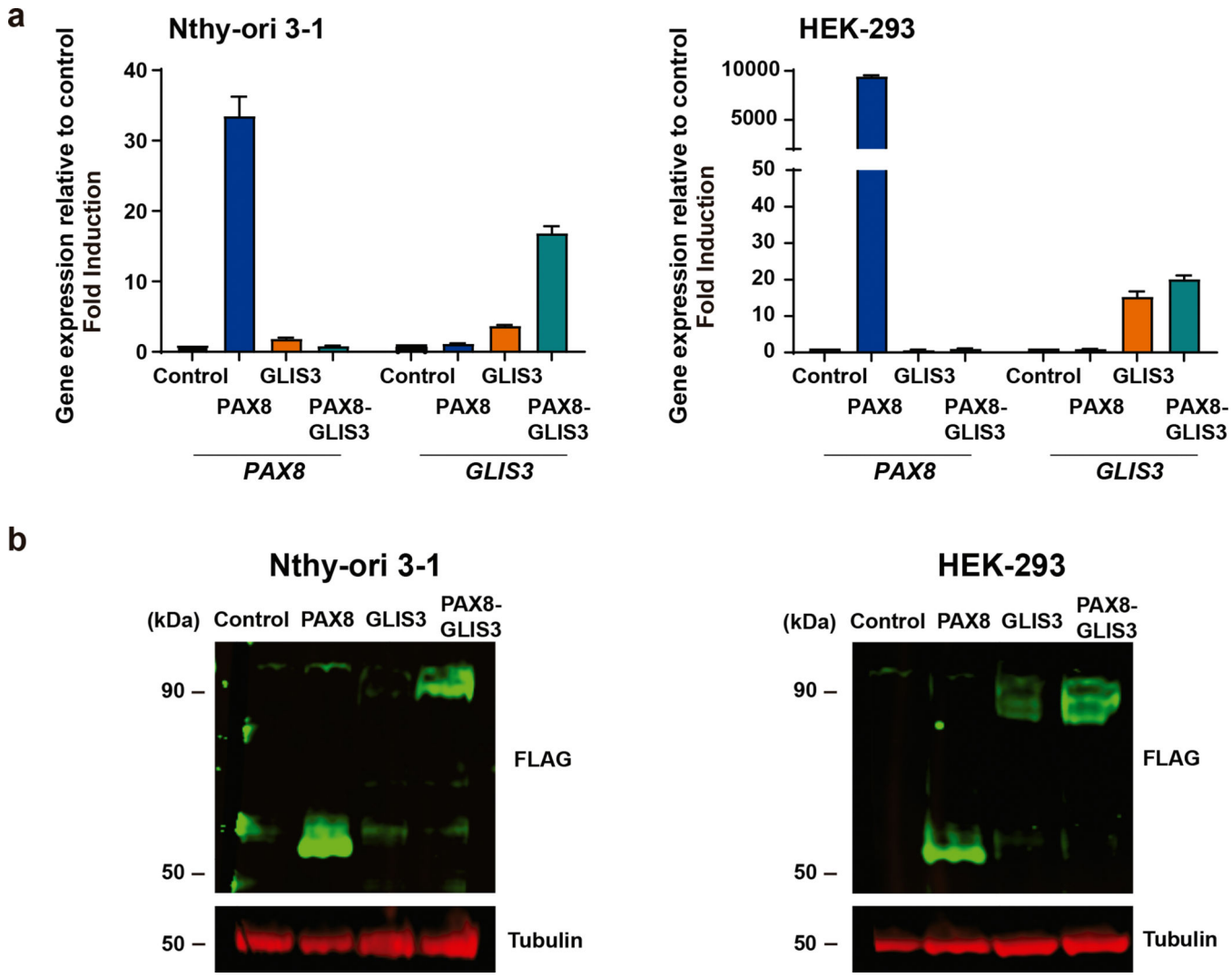

Figure 1: PAX8-GLIS3 expression in Nthy-ori 3–1 and HEK-293 cell lines.

(a) Quantitative RT-PCR analysis of *PAX8* and *GLIS3* gene expression in Nthy-ori 3–1 and HEK-293 cells expressing empty vector (Control), wild-type (WT) PAX8 (PAX8), WT GLIS3 (GLIS3) or the PAX8-GLIS3 fusion. *GAPDH* was used as endogenous control. (b) Representative western blot analysis of FLAG protein expression in Nthy-ori 3–1 and HEK-293 cells expressing Control, PAX8, GLIS3 or PAX8-GLIS3. The flag-tagged proteins migrate according to their predicted molecular weights (50 kDa for PAX8, 100 kDa for GLIS3 and 90 kDa for PAX8-GLIS3). Tubulin was used as protein loading control. All experiments were performed in triplicate. Error bars, mean ± SEM.

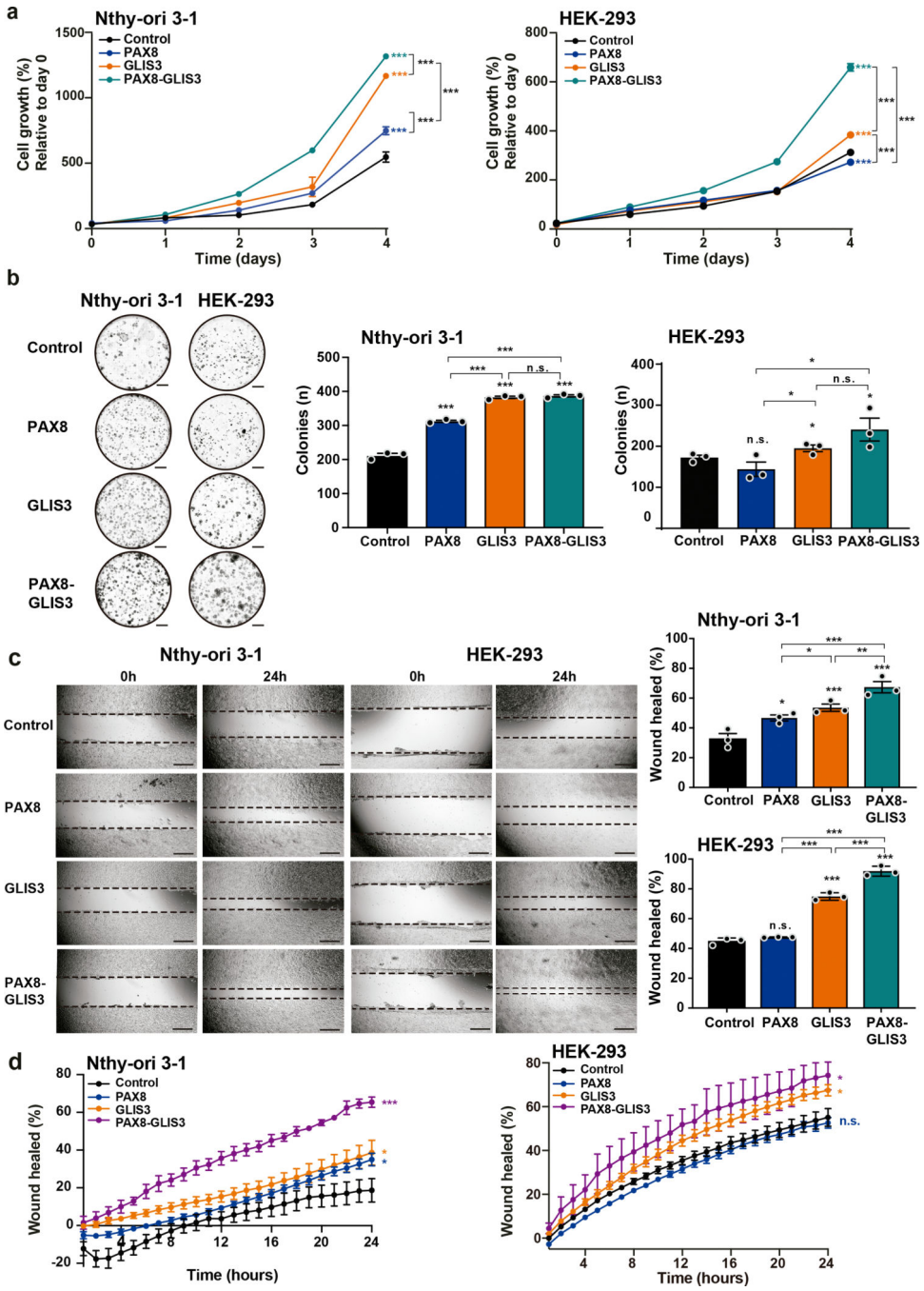

Figure 2: PAX8-GLIS3 expression results in acquisition of oncogenic properties *in vitro*.

(**a**) Proliferation assay of Nthy-ori 3–1 and HEK-293 cells expressing empty vector (Control), wild-type (WT) PAX8 (PAX8), WT GLIS3 (GLIS3) or PAX8-GLIS3 fusion, performed over 5 days. (**b**) Colony formation assay of Nthy-ori 3–1 and HEK-293 cells with stable transduction of control, PAX8, GLIS3 or PAX8-GLIS3. Scale bars, 5 mm. Quantification (right) of number of colonies/well compared to control. (**c**) Wound healing assay of Nthy-ori 3–1 and HEK-293 cells expressing Control, PAX8, GLIS3 or PAX8-GLIS3. Wound area was assessed at 0 and 24 h. Scale bar, 500 μm. Quantification (right) of

wound healed compared to control. (**d**) Quantification of time-lapse wound healing assay of Nthy-ori 3–1 and HEK-293 cells expressing Control, PAX8, GLIS3 or PAX8-GLIS3. Wound area was assessed every hour during the course of 24 h. All experiments were performed in triplicate. Error bars mean ± SEM; n.s., not significant; * $P<0.05$, ** $P < 0.01$, *** $P < 0.001$; two-tailed unpaired t-test.

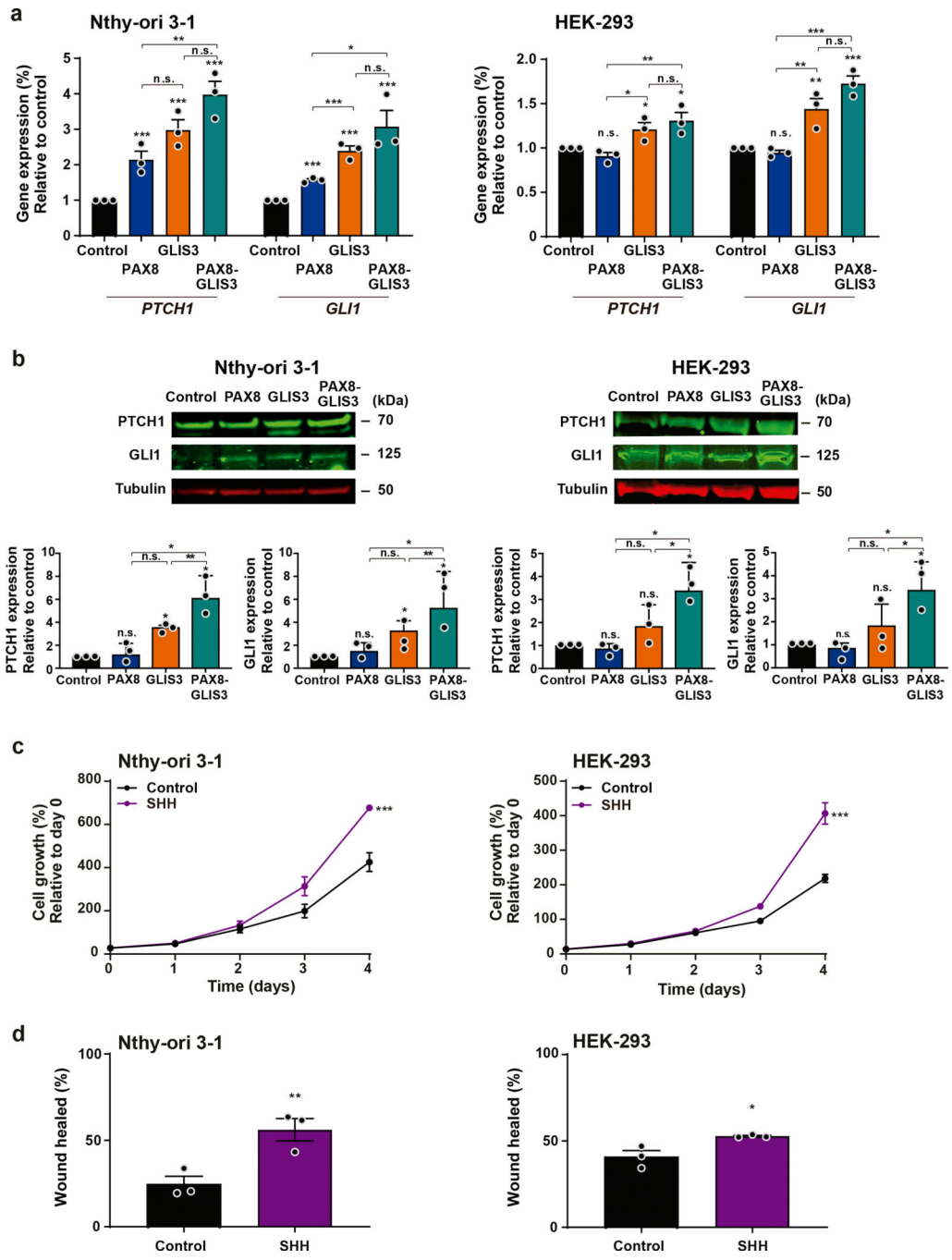

Figure 3: PAX8-GLIS3 expression results in Sonic Hedgehog pathway activation.

(**a**) Quantitative RT-PCR analysis of *PTCH1* and *GLI1* in Nthy-ori 3–1 and HEK-293 cells expressing empty vector (Control), wild-type (WT) PAX8 (PAX8), WT GLIS3 (GLIS3) or PAX8-GLIS3 fusion. *GAPDH* was used as endogenous control. (**b**) Representative western blot analysis of PTCH1 and GLI1 protein expression in Nthy-ori 3–1 and HEK-293 cells expressing control, PAX8, GLIS3 or PAX8-GLIS3 fusion. Tubulin was used as protein loading control. Quantification (below) of protein expression compared to control. (**c**) Proliferation assay of parental Nthy-ori 3–1 and HEK-293 cells treated with human

recombinant SHH Protein at 1 μg/ml or vehicle (Control) performed over 5 days. (**d**) Quantification of the wound healing assay of parental Nthy-ori 3–1 and HEK-293 cells treated with SHH Protein at 1 μg/ml or control. All experiments were performed in triplicate. Error bars, mean ± SEM; n.s., not significant; *P < 0.05, ** P < 0.01, *** P < 0.001; two-tailed unpaired t-test.

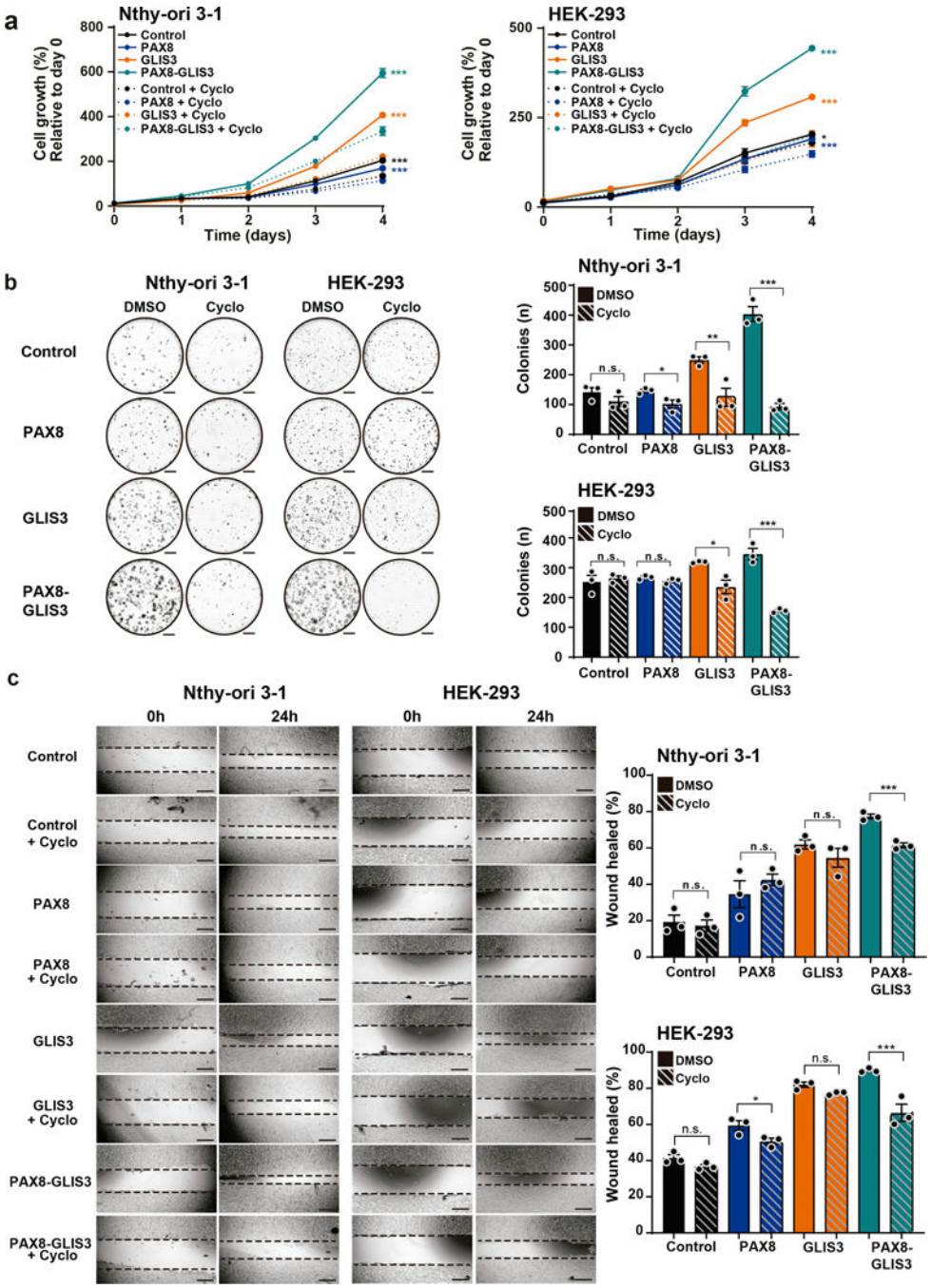

Figure 4: Reversal of oncogenic properties in *PAX8-GLIS3* fusion gene expressing cells upon inhibition of the Sonic Hedgehog pathway.

(**a**) Proliferation assay of Nthy-ori 3–1 and HEK-293 cells expressing empty vector (Control), wild-type (WT) PAX8 (PAX8), WT GLIS3 (GLIS3) or PAX8-GLIS3, treated with Cyclopamine at 10 μM or vehicle control (DMSO) performed over 5 days. (**b**) Colony formation assay of Nthy-ori 3–1 and HEK-293 cells with stable transduction of Control, PAX8, GLIS3 or PAX8-GLIS3 treated with Cyclopamine at 10 μM or vehicle control (DMSO). Scale bars, 5 mm. Quantification (right) of number of colonies/well compared to

control. (**c**) Wound healing assay of Nthy-ori 3–1 and HEK-293 cells expressing Control, PAX8, GLIS3 or PAX8-GLIS3 treated with Cyclopamine at 10 μM or vehicle control (DMSO). Wound area was assessed at 0 and 24 h. Scale bar, 500 μm. Quantification (right) of wound healed compared to control. Cyclopamine (Cyclo). All experiments were performed in triplicate. Error bars, mean ± SEM.; n.s., not significant; * $P<0.05$, ** $P < 0.01$, *** $P < 0.001$; two-tailed unpaired t-test.

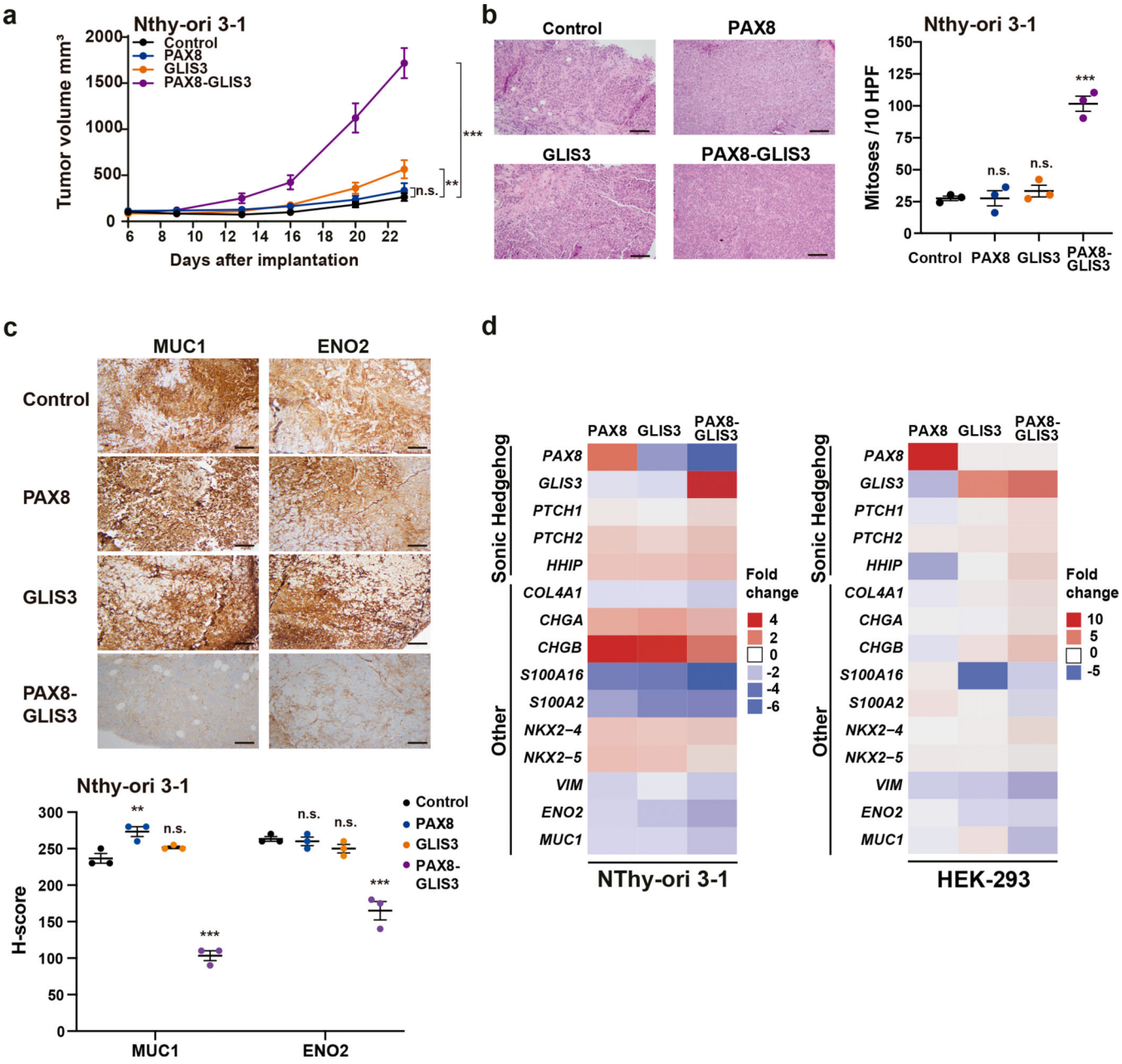

Figure 5: Tumorigenicity assessment by xenograft assay and differential gene expression analysis.

(**a**) Tumor growth (volume mm^3) from xenograft tumor derived from Nthy-ori 3–1 cells expressing empty vector (Control), wild-type (WT) PAX8 (PAX8), WT GLIS3 (GLIS3) or PAX8-GLIS3. All conditions were compared to Control. (**b**) Representative hematoxylin-and-eosin micrographs of xenograft tumor derived from Nthy-ori 3–1 cells expressing Control, PAX8, GLIS3 or PAX8-GLIS3. Scale bars, 50 μm. Quantification (right) of mitoses per 10 high power fields (HPF). (**c**) Representative immunohistochemical micrographs of MUC1 and ENO2 in xenograft tumors derived from Nthy-ori 3–1 cells expressing Control, PAX8, GLIS3 or PAX8-GLIS3. Scale bars, 50 μm. H-score assessment (below). (**d**) Differential gene expression analysis of Nthy-ori 3–1 and HEK-293 cells expressing PAX8,

GLIS3 or PAX8-GLIS3 subjected to RNA-sequencing. Gene expression fold-change, relative to the gene expression levels in Nthy-ori 3–1 or HEK-293 cells expressing empty vector, is color-coded according to the legend. Experiments were performed in triplicate. Error bars, mean ± SEM; n.s., not significant; *P < 0.05, ** P < 0.01, *** P < 0.001; two-tailed unpaired t-test.